Int. J. Electrochem. Sci., 14 **(2019)** 8869 – 8881, doi: 10.20964/2019.09.19

International Journal of
ELECTROCHEMICAL
SCIENCE
www.electrochemsci.org

Preparation of g-C_3N_4/ $Zn_3In_2S_6$ Composite Materials as Photocatalysts for the Highly Efficient Degradation of Antibiotic

Kuan Chen[1,2], Tianhong Xu[2], Hongjian Xu[1,2,], Qiang Wu[1,2,*], Weiguo Pan[3]*

[1] Shanghai Key Laboratory of Materials Protection and Advanced Materials in Electric Power, Shanghai University of Electric Power, Shanghai, 200090, P.R. China.
[2] Department of Environmental and Chemical Engineering, Shanghai University of Electric Power, Shanghai,200090, P.R. China
[3] Department of Energy Source and Mechanical Engineering, Shanghai University of Electric Power, Shanghai,200090, P. R. China
[*]E-mail: hongjian_xu@sina.com, qiangwu@shiep.edu.cn

Received: 8 My 2019 / *Accepted:* 26 June 2019 / *Published:* 31 July 2019

We designed and succeeded in synthesising a sequence of g-C_3N_4/$Zn_3In_2S_6$ (ZIS) composite photocatalysts by means of one-step hydrothermal synthesis, which integrated different amounts of g-C_3N_4 into ZIS. The prepared products are characterized by means of various characterization methods to determine their structure, morphology and physicochemical properties. Their photocatalytic activities were assessed according to the performance of tetracycline ($C_{22}H_{24}N_2O_8$, TC) degradation experiments with light radiation. This consequence of experiments showing that the g-C_3N_4 (0.5 wt.%)/ZIS photocatalyst is most effective for the photodegradation of TC. Moreover, results from the cyclic tests confirm the stability of the g-C_3N_4 (0.5 wt.%)/ZIS composite, which remained active after five cycles of repeated photocatalysis experiments. We can get the conclusion that $\bullet O_2^-$, •OH and h^+ all played roles during the degradation process from the figures of ESR tests and active species trapping experiments. And the corresponding degradation mechanism of g-C_3N_4/ZIS composites is proposed. High specific surface areas, desirable absorption capability, suppression of charge recombination should be put down to its nice photocatalytic performance. Thus, it can be considered that g-C_3N_4/ZIS composites have broad potential application prospects in photocatalysis degradation.

Keywords: $Zn_3In_2S_6$, degradation, g-C_3N_4, TC, photocatalytic

1. INTRODUCTION

Water pollution caused by industry and medicine has become a huge challenge facing the world. [1-3] Antibiotics as a relatively large amount of drugs have seriously affected human health and ecosystems. [4,5] Antibiotic wastewater with high chemical oxygen demand, unstable water quality and

a large amount of inhibitory substances, which has always been a difficult point in wastewater treatment [6-10]. Therefore, finding a green simple and efficient means to remove antibiotics in water has become the focus of researchers. Photocatalytic oxidation technology has become one important avenue in water treatment because of its simplicity, environmental protection, high efficiency, stability [11,12]. The exploitation of new semiconductor materials has attracted worldwide attention.

Semiconducting neoteric ternary oxide Zn-In-S has recently drawn considerable attention in virtue of their peculiar and superior electrical and photocatalytic properties [13-15]. Lei *et al*. [16] demonstrated the fabrication of $ZnIn_2S_4$ nanoparticles and the application for hydrogen production on the irradiating condition of visible light. Jiang *et al*. [17] synthesized double shell $ZnIn_2S_4$ nanosheets/TiO_2 hollow nanosphere to improve the photocatalytic activities. Zhang *et al*. [18] have prepared a $Zn_3In_2S_6$@ZnO photocatalyst which could selective oxidize benzyl alcohol to benzaldehyde. Nevertheless, it also should be pointed out that the catalytic performance of $Zn_3In_2S_6$ is not satisfactory, for its sluggish isolation efficiency and weak ability on the charge carrier's migration. Thus, the active search for efficient, stable and unique $Zn_3In_2S_6$-based materials will become a hot research topic.

Recently noted that graphite carbonitride (g-C_3N_4) has good versatility, for example photochemical stability, easy synthesis and low cost [19-22], has aroused great interest among scholars in the field of photocatalysis and materials science [23-26]. However, less ideal photocatalytic performance of g-C_3N_4 has become an obstacle to its practical application. The photocatalytic efficiency also can be improved by preparing a g-C_3N_4 based composite photocatalyst [27-29].

Got inspiration from these creative ideas, we firstly and successfully synthesized a series of $Zn_3In_2S_6$ microspheres decorated with small quantity of g-C_3N_4 through a hydrothermal route that can be easily operated [30]. And we employed Tetracycline ($C_{22}H_{24}N_2O_8$, TC) as a model dye to monitor the activity of materials for photocatalytic degradation. Tetracycline (TC) as a most widely used antibiotics in humans or animals. And the great mass of TC goes into the natural except for a small amount of tetracycline absorbed by the body. The residual of TC could have a serious impact on the environment. The stability test experiment of the catalysts was also performed. Above all, it may provide new these finding for designing novel composites with multi-functional applications according to these findings.

2. EXPERIMENTAL

2.1 Reagents

All chemicals were of analysis reagent grade. Indium nitrate hydrate ($In(NO_3)\cdot 6H_2O$), Zinc chloride ($ZnCl_2$) and thioacetamide (C_2H_5NS) were purchased from Aladdin. Ethanol (C_2H_5OH), 1,3,5-Triazine-2,4,6-triamine ($C_3H_6N_6$, Melamine) and Tetracycline ($C_{22}H_{24}N_2O_8$, TC) were purchased from Tansoole. Deionized and doubly distilled water was home-made in the laboratory.

2.2 Synthesis of Different Catalyst

g-C_3N_4 was firstly produced from calcining melamine by a two-step heat treatment; Firstly,

weighed a certain amount of melamine into the small porcelain boat and placed them in a Muffle furnace, heat up to 773 K for 2 h in air at a heating rate of 2 °C/min and then heat up to 793 K at a heating rate of 2 °C/min for 2 h for deamination, lastly, keeping the sample cool down naturally. Secondly, the above sample is ground and placed in a muffle furnace again at a heating rate of 2 °C/min to a temperature of 793 K for 6 h, and naturally cooled to obtain a two-dimensional ultra-thin g-C_3N_4.

By doping different wt.% g-C_3N_4 into ZIS microsphere with a hydrothermal method to prepare a battery of g-C_3N_4/ $Zn_3In_2S_6$ composites; First, accurately weigh $In(NO_3)_3 \cdot 6H_2O$ (4 mmol), $ZnCl_2$ (6 mmol) and dispersed them into a 80ml solution which contained excess of C_2H_5NS; whereafter, adding 0~2 wt.% g-C_3N_4 into the mixture. The hybrid products were named according to their g-C_3N_4 content (m wt.%)/ZIS (m=0, 0.25, 0.5, 1, 2). The resulting solution was then sonicated for half an hour and stirred for 2 h. Lastly, shifted the mixed solution to a Teflon-lined autoclave and take a hydrothermal reaction process at 453 K for 12 h; keep the reactor cooling naturally at the end of the reaction. The homologous specimens were gathered after centrifugation, rinsed with ethanol and deionized water, repeated three times, kept dry at 333 K for 10 h to obtain the g-C_3N_4 (m wt. %) /ZIS composite. The sample with m=0 was named ZIS.

2.3 Photocatalyst Characterization

X-ray diffraction (XRD) patterns of materials was acquired on an ADVANCE-D8 diffractometer. The structure and morphology were acquired by scanning electron microscope instrument (SEM, Hitachi SU-1500) and transmission electron microscope instrument (TEM, JEM-2010). UV-visible diffuse reflectance spectroscopy (Shimadzu UV-2550) was collected on the wavelength between 200 nm and 800 nm. X-ray photoelectron spectroscopy (XPS) of the composites was carried using an ESCALAB250Xi photoelectron spectrometer. The specific surface area was evaluated by the plot of N_2 adsorption isotherms recorded on a Quantachrome Autosorb-1 instrument. Electron spin resonance spectroscopy (ESR) identification of active materials using a Bruker EPR A300-10/12 spectrometer.

2.4 Photoelectrochemical Tests

The electrochemical and photoelectrochemical tests were operated on a three-electrode structure, based on a CHI660E electrochemical workstation (CHI instruments) [31]. The electrolyte for the photoelectrochemical measurements was Na_2SO_4 aqueous solution (0.2 M). The counter electrode and reference electrode were selected as a large Pt wire and a saturated calomel electrode (SCE), respectively [32]. The preparation of working electrode was by the following process: took 20 mg photocatalyst sample dissolved in 1 mL ethanol and 10 μL Nafion, and following sonicated for 30 min. A fixed area of 1×1cm^2 on the glassy carbon electrode (GCE) was smeared with 20 μL of the suspension. The electrochemical impedance spectroscopy (EIS) analysis was measured by CHI660E electrochemical workstation.

2.5 Study on Photocatalytic Performance

In this degradation experiments, the TC solution was put into a self-made reactor. And the temperature was controlled through recycled water. Use 300W full-spectrum xenon lamp as the source of UV-visible light. Briefly, 50 mg of the different g-C_3N_4/ZIS catalysts was first suspended in 100 mL TC solution whose concentration was 10 mg/L. Then, kept the suspension solution stir continuously until adsorption-desorption equilibrium ahead of light irradiation. At fixed time intervals, took 4 mL- sample for a 5 min centrifugation at 10000 rpm, the survived level of TC was analysed with UV-vis spectrophotometer at 554 and 463 nm of the maximum adsorptive wavelength. The removal efficiency (A%) of TC over the photocatalyst was got according to the following equation:

$$A\% = \frac{C_0 - C_t}{C_0} \times 100\% \quad (1)$$

Where C_0, C_t respectively representing the fresh and the instantaneous concentration at a given intervals (t) during the degradation reaction.

3. RESULTS AND DISCUSSION

3.1 Physicochemical Features and Electrochemical Measurements

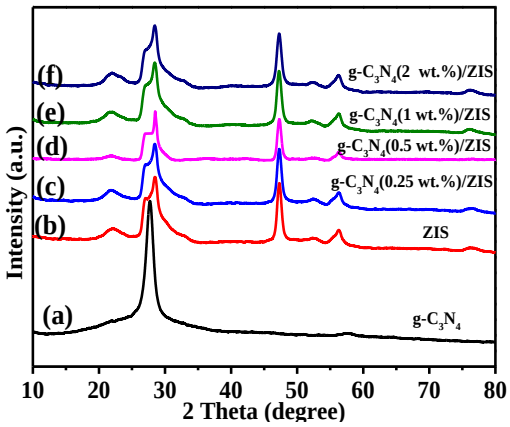

Figure 1. XRD patterns of the as-prepared series $Zn_3In_2S_6$ composites and g-C_3N_4

Figure 1 shows the XRD diffraction pattern of pure g-C_3N_4, ZIS and its g-C_3N_4/ZIS composites. XRD data in Fig. 1a shows a typical broad diffraction peak centred at 27.4°, corresponding to the (002) plane for bulk g-C_3N_4 (JCPDS Card No. 50-1512). As shown in Fig. 1b, the diffraction peaks of samples keep in line with those of $Zn_3In_2S_6$ (JCPDS No. 65-4003) with a typical hexagonal structure, which was reported previously. [18]. Moreover, the different as-prepared g-C_3N_4/ZIS composites exhibit similar XRD patterns (Fig. 1c-1f) with diffraction peaks originating from both g-C_3N_4 and ZIS. The intensity of the characteristic diffraction peak of g-C_3N_4 in g-C_3N_4/ZIS composite materials is not obvious, because the doping amount is relatively low. Also, no peaks from any other phases are observed, indicating that no impurities are present in the g-C_3N_4/ZIS composites.

We further studied the morphology and structure of pure g-C_3N_4, ZIS and its g-C_3N_4/ZIS

composite materials by Scanning electronic microscopy (SEM) and transmission electron microscope (TEM). Fig. 2a-2b are the typical SEM and TEM images of g-C_3N_4, actually, it is a two-dimensional thin layer. ZIS shows a uniform microsphere-like morphology with a diameter of 400 nm, and the surface of these microspheres display wool shape which caused higher surface area and the increasement of active sites (Fig. 2c). SEM image of g-C_3N_4 (0.5 wt.%)/ZIS (Fig. 2d) shows that microsphere-shaped ZIS is wrapped by a two-dimensional thin layer of g-C_3N_4. Moreover, Fig. 2e indicate the presence of all the constituting elements (C, Zn, In, S and N), confirming the successful synthesis of g-C_3N_4/ZIS composites.

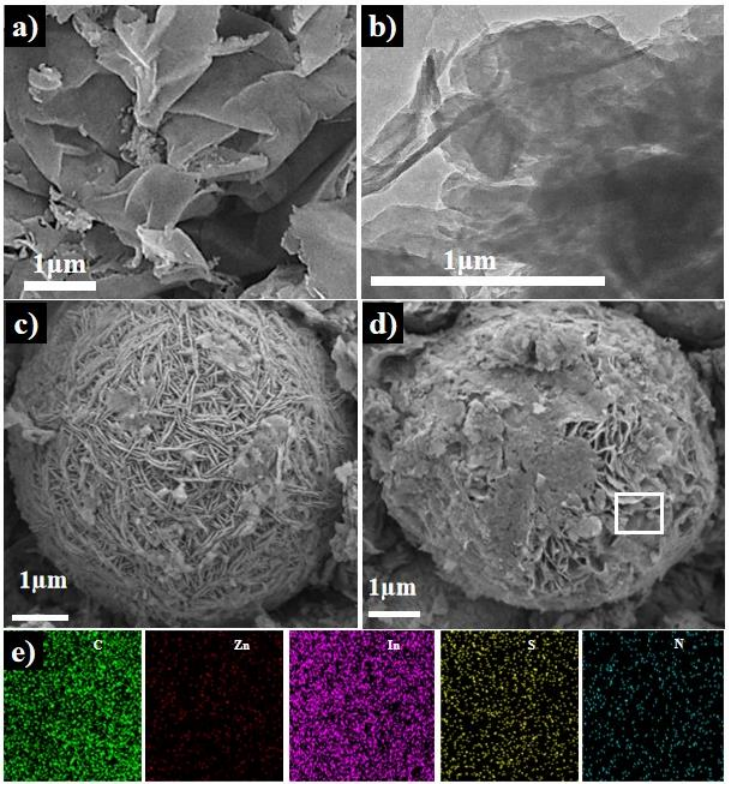

Figure 2. SEM images of (a) g-C_3N_4, (c) ZIS and (d) g-C_3N_4 (0.5 wt.%)/ZIS; TEM image of (b) g-C_3N_4 and (e) elemental mapping analysis of g-C_3N_4 (0.5 wt.%)/ZIS

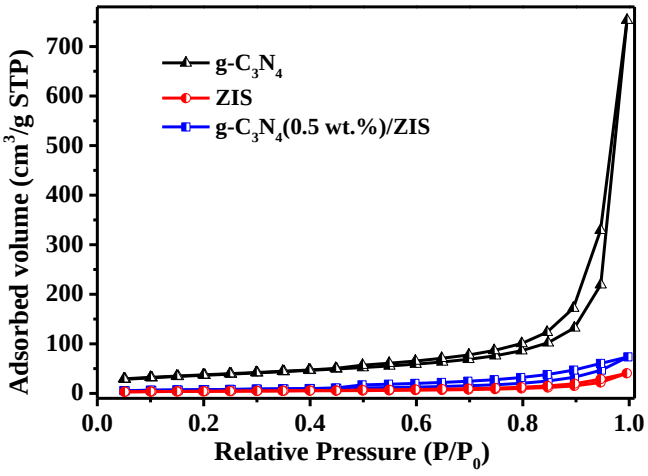

Figure 3. N_2 adsorption-desorption isotherms

Nitrogen adsorption-desorption analysis was estimated the special surface area of composites. All the isotherms in Fig. 3 show a type IV loop, as per IUPAC classification [33], implying a microporous structure for $Zn_3In_2S_6$ and the composites. The surface areas of g-C_3N_4, $Zn_3In_2S_6$ and g-C_3N_4 (0.5 wt.%)/ZIS were calculated to be 127.8 m^2/g, 88.648 m^2/g and 95.806 m^2/g, corresponding. Compared with pure ZIS, it is clearly the increased area of g-C_3N_4 (0.5 wt.%)/ZIS. We can thus conclude that the addition of g-C_3N_4 may enhance specific surface area and prompt the photocatalytic activity.

XPS spectrum was performed to ulterior research the component element analysis and valence states of g-C_3N_4 (0.5 wt.%)/ZIS hybridization; results were shown in Fig. 4. The clear presence of photoelectron lines at binding energies (EB) of ca. 162 eV, 284 eV, 398 eV, 445 eV, and 1022 eV in Fig. 4a further confirmed the presence of S, C, N, In and Zn elements, respectively. As displayed in Fig. 4b, at 284.8, 287.4, 289.6eV, there are peaks which can be put down to C-C, C-N, N-C=N bonds, responsively. Two peaks, seen in the S 2p spectra (Fig. 4c), matched well with S $2p_{3/2}$ (161.7 eV) and S $2p_{1/2}$ (162.9 eV) [34]. It indicated that the valence state of In is +3 from the Fig. 4d which shown a doublets at 444.9 eV and 452.5 eV [35,36]. The peak of Zn^{2+} $2p_{3/2}$ and $2p_{1/2}$ are corresponding to 1022.1 and 1045.2 eV (Fig. 4e) [37]. The two peaks of N 1s spectrum were corresponding with C-N-C (397.89V), N-$(C)_3$ (401.2 eV) [31]. Hence, from XPS data, we infer that composites were successfully synthesized from pure ZIS and g-C_3N_4.

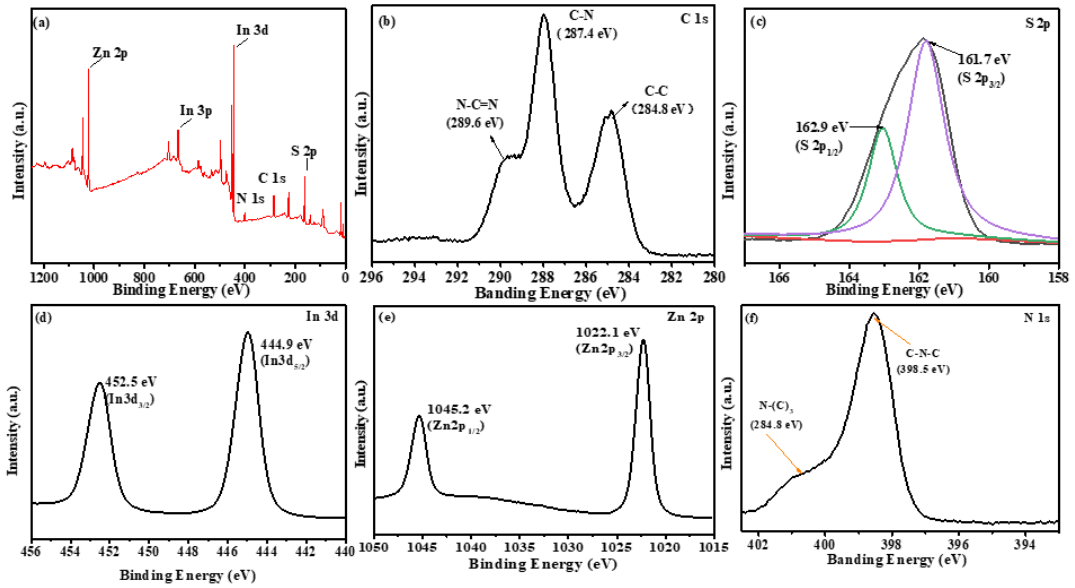

Figure 4. XPS spectra of g-C_3N_4 (0.5 wt.%)/ZIS: (a) survey of the sample, (b) C 1s, (c) S 2p, (d) In 3d, (e) Zn 2p and (f) N 1s

The samples' light absorption capability was revealed by UV-Vis spectrum (UV-Vis DRS) (Fig. 5). Notably, the g-C_3N_4/ZIS composites display a stronger absorption during UV region than ZIS, own to absorption by g-C_3N_4. Specially, the absorption intensity was significantly improved by decorating the surface of ZIS microspheres with a little amount (0.5 wt.%) of g-C_3N_4, which is beneficial to promoting the photocatalytic activity. Therefore, it can be reasonable to believe that g-C_3N_4 (0.5 wt.%)/ZIS has a favorable application prospect in photocatalytic degradation of pollutants.

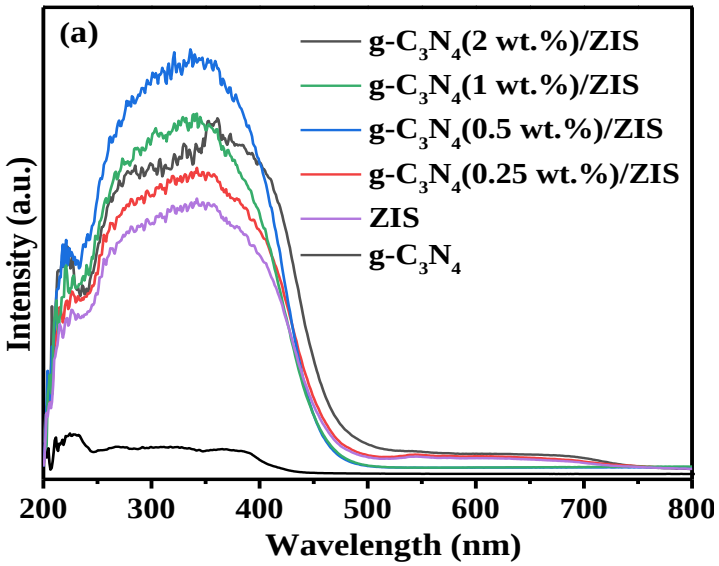

Figure 5. UV-vis absorption spectra of pure g-C_3N_4, ZIS, various composite

3.2 Degradation Activity Test

3.2.1 Impact of g-C_3N_4 doping content

The degradation curve of TC on the various g-C_3N_4/ZIS hybrids was displayed in the Fig. 6a, noted that we also conduct the pure $Zn_3In_2S_6$, g-C_3N_4 and the blank experiment (direct photolysis without any catalyst) for comparison. From the image, we can clearly get that the efficiency of the blank experiment was only ca.4.7%. The removal efficiency for TC over samples are list in descending order of g-C_3N_4 (0.5 wt.%)/ZIS, g-C_3N_4 (1 wt.%)/ZIS, g-C_3N_4 (2 wt.%)/ZIS, g-C_3N_4 (0.25 wt.%)/ZIS, pure ZIS and fresh g-C_3N_4. Obviously, the concentration of TC dye decreased to zero during 25 min for all the composites which showing superior performance relative to fresh g-C_3N_4 and $Zn_3In_2S_6$. According to the results of experimental data, we conclude that too low doping amount of g-C_3N_4 is not conducive to providing enough active sites for the ZIS, and too high doping amount makes g-C_3N_4 occupy the active sites on the surface of ZIS. The results implied the photocatalytic performance could be enhanced through doping appropriate g-C_3N_4 into $Zn_3In_2S_6$ and the optimum amount of g-C_3N_4 is 0.5 wt.%. Therefore, the exploration experiment of others conditional optimization was based on the model photocatalytic degradation over g-C_3N_4 (0.5 wt.%)/ZIS.

3.2.2 Impact of primal TC concentrations

To evaluate the influence for photocatalytic degradation efficiency over original TC concentrations. We choose g-C_3N_4 (0.5 wt.%)/ZIS as a model for the degradation experiment under various of initial TC concentrations. Results shown in Fig. 6b, the adsorbing workpiece ratio under darkness was 14.9%, 7.29%, 4.64% and 5.169% at the corresponding original TC concentration with 5, 10, 15 and 20 mg/L. The sample of original TC concentration at 5 and 10 mg/L were completely

degraded in the next 10 and 15 minutes with the xenon lamp irradiation and the others were completely degraded after 20 min. Their corresponding photocatalytic degradation efficiency was calculated to 85.1%, 92.8%, 95.4% and 94.8%. The experimental results show that the photocatalytic degradation efficiency of g-C_3N_4 (0.5 wt.%)/ZIS increases with the increase of TC concentration in a certain range, and the amount of adsorbed TC in the dark reaction decreases gradually. The reason may be that with the increase of TC concentration, the photon path length into TC solution will decrease, thereby reducing the photocatalytic efficiency. In addition, TC molecule may generate other intermediates in the photocatalytic process, and then compete with TC molecule for adsorption and photocatalytic sites on the catalyst surface. Synthesizes both dark and irradiation possess performance, we can get the conclusion that the primal TC concentration hold the balance on the process of degradation. Took it all together, we adopt TC solution (10 mg/L) in a follow-up degradation experiment. Meanwhile, we have collected some other literatures about photocatalytic degradation of tetracycline and the results were listed in Table 1. It can be clearly seen that g-C_3N_4 (0.5 wt.%)/ZIS has the highest photocatalytic ability to degrade TC.

3.3 Recyclability and stability of g-C_3N_4 (0.5 wt.%)/ZIS composites

Other than above the photoactivity, the stability is another momentous element to judge the photocatalyst whether suitable for the practical applications. Five cycles experiment was researched over g-C_3N_4 (0.5 wt.%)/ZIS composites under the same conditions. After each cycle, the g-C_3N_4 (0.5 wt.%)/ZIS sample was gathered after centrifugation, rinsed by ethanol and deionized water, repeated three times, and drying. Fig. 6c shows that after five successive cycles, the degradation efficiency is reduced by just 10%. The reason for this reduction in efficiency could be due to loss of catalyst sample during the collection of the recycled catalyst. Additionally, as Fig. 6d demonstrated, no obvious differences are observed in XRD patterns of g-C_3N_4 (0.5 wt.%)/ZIS composite used five times and the fresh sample. Based on these results, we conclude that g-C_3N_4 (0.5 wt.%)/ZIS composite is a stable and high-efficiency photocatalyst.

3.4 Study on Photocatalytic Principle

3.4.1 Photoelectrochemical peculiarity research

To account for the remarkable photocatalytic performance of g-C_3N_4 (0.5 wt.%)/ZIS on TC, we have performed three times photo-electrochemical experiments. Fig. 7a acted the photocurrent-time graph of single g-C_3N_4, $Zn_3In_2S_6$ and g-C_3N_4 (0.5 wt.%)/ZIS composites for several on-off cycles. It can be seen that with the light was switched on or turn off, the photocurrent density fast rising and immediately decline to its initial value, respectively. The g-C_3N_4 (0.5 wt.%)/ZIS composite exhibited super stabilities with its unchanged peak values and a highest photocurrent intensity than the pure g-C_3N_4 and ZIS. Of which generally accepted point was that with the light irradiation, the diffusion electrons separated from the electron-hole pairs, the photocurrent came into being. Thus, we can infer

that g-C_3N_4 (0.5 wt.%)/ZIS composites promotes separation and transformation for the photoexcited electron-hole pairs should be put down to the decoration of g-C_3N_4.

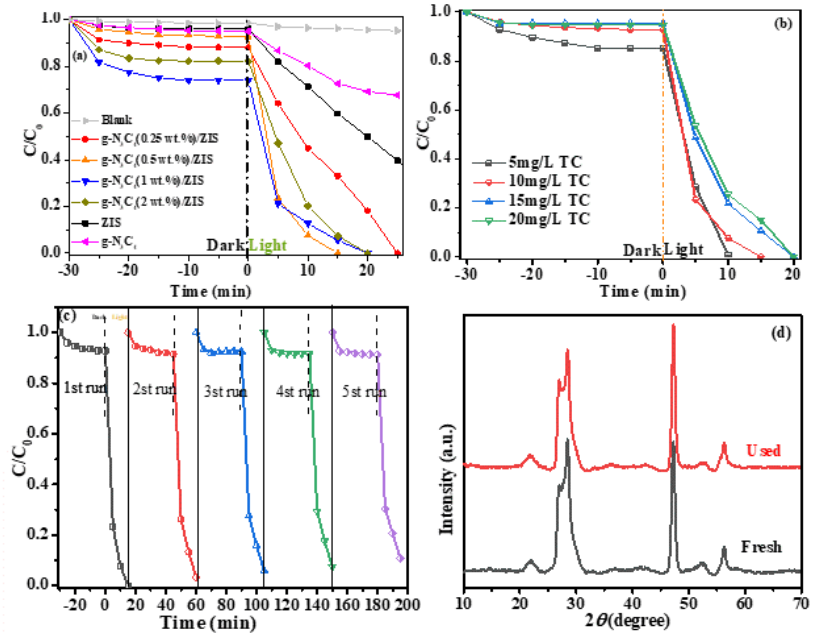

Figure 6. (a) Plots of TC degradation over various g-C_3N_4 amount on the ZIS, (b) degradation performance over g-C_3N_4 (0.5 wt.%)/ZIS in different concentrations solution of TC, (c) Photocatalytic degradation over 5 cycles; (d) XRD patterns before and after degradation

Table 1. Comparison of the photocatalytic performance of g-C_3N_4 (0.5 wt.%)/ZIS with other photocatalysts in the reported literatures.

photocatalysts	m_{Cat} (mg/L)	t(min)	Con. (%)	ref.
ZIS/TiO_2-2	10	80	82.74	[17]
ZIS/CQDs-2	10	50	85.07	[38]
BWO-CBO-5	15	60	90	[39]
g-C_3N_4(0.5wt%)/ZIS	10	15	100	this work

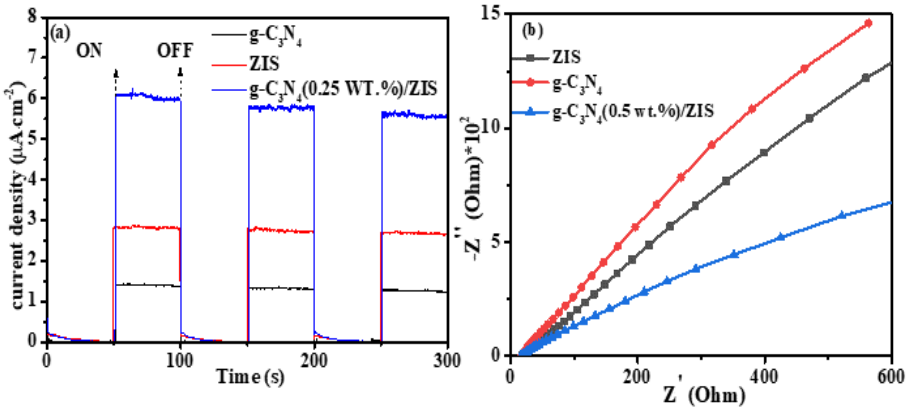

Figure 7. (a) Photocurrent pattern and (b) EIS analysis of samples

Meanwhile, electrochemical impedance spectra (EIS) test gained further analysis into the transfer and recombination efficiency of the charges [38-40]. The resistance value of photocatalyst keeps line with the arc radius in EIS image. Generally speaking, the smaller radius, the smaller resistance value. As shown in Fig. 7b, g-C_3N_4 (0.5 wt.%)/ZIS composite displayed the smallest arc radius among these samples in the EIS Nyquist plot, indicating that this composite has the lowest electrical resistance, the superior transfer ability of charge and the corresponding electron-hole pairs separated most efficiently. This result is in accordance with the observed trend in photocurrent response.

3.4.2 Role of reactive species

To further study the electron transfers mechanistic information during the degradation reaction over ZIS compounds, the capture experiment was performed and the main oxidative species ($\bullet O_2^-$, •OH, and h^+) were detected by BQ, IPA and EDTA, respectively [41-43]. As depicted in Fig. 8a, when IPA was introduced into the reaction, the efficiency was not decrease obviously indicating that •OH scarcely interferes with the degradation of TC. But it had a noteworthy reduction after adding BQ, which implying $\bullet O_2^-$ had a great impact on the catalysis degradation process. Furthermore, a similar phenomenon occurred after adding EDTA into the solution means another crucial active species is h^+. Therefore, we can draw a conclusion that $\bullet O_2^-$ and h^+ took a primary responsibility and •OH influenced scarcely on the TC removal.

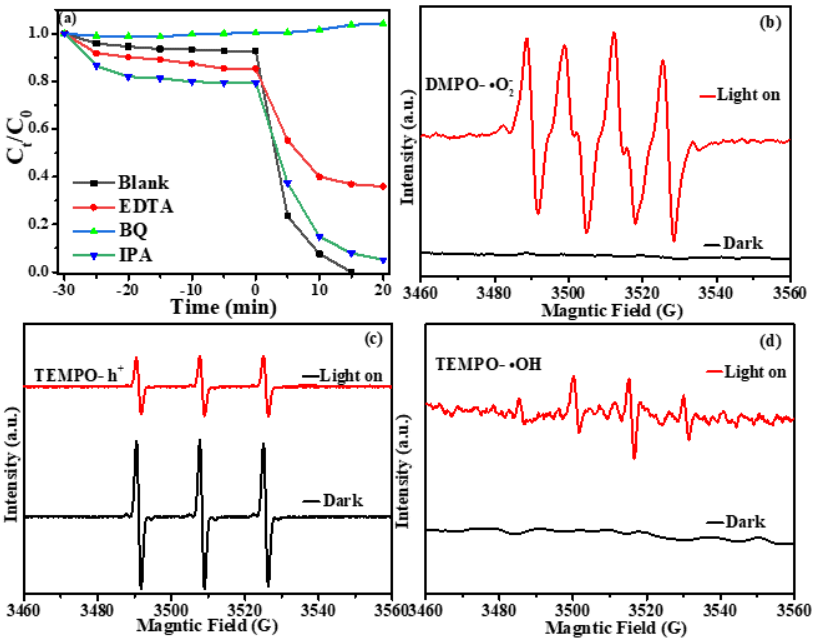

Figure 8. (a) photocatalytic activities of g-C_3N_4 (0.5 wt.%)/ZIS with different scavengers, ESR images of the DMPO-$\bullet O_2^-$ (b), TEMPO-h^+ (c) and TEMPO-•OH (d) for g-C_3N_4 (0.5 wt.%) under darkness and irradiation.

ESR analysis are displayed in Fig. 8b-d. The distinct specific signals of DMPO-$\bullet O_2^-$ (Fig. 8b)

were detected under irradiation compared with that curve under darkness. And the characteristic peaks of TEMPO-h^+ are also perceived (Fig. 8c), the intensities of the peaks sharply decreased under irradiation are correlated with that in the dark for g-C_3N_4 (0.5 wt.%)/ZIS. As shown in Fig. 8d, there is a negligible peak intensity of the DMPO-•OH during darkness and after longer duration of full spectrum irradiation, bits of characteristic peaks and corresponding troughs emerged, indicating that •OH was also contributing to the photocatalytic process. Hence, Base on the above analysis, one can draw a conclusion that the process of TC degradation was a consequence of •O_2^-, h^+ and •OH working together.

3.5 Proposed photocatalytic mechanism

As described in Fig. 9, a conceivable degradation route of g-C_3N_4 (0.5 wt.%)/ZIS composites photocatalyst is proposed. We note that CB potential of g-C_3N_4 and $Zn_3In_2S_6$ are -1.37 V and -0.56 V. When the g-C_3N_4 (0.5 wt.%)/ZIS composite is irradiated, the electrons both activated from VB to CB in ZIS and g-C_3N_4, leaving holes in VBs. Photo-excited electrons can quickly shift from the g-C_3N_4 to ZIS on the CB. On the other hand, the photogenerated holes on the VB of ZIS can move to that of g-C_3N_4. Because g-C_3N_4 has a more negative CB potential than the O_2/• O_2^- (-0.046 V). The accumulated electrons will be trapped by the dissolved oxygen to produce to • O_2^- on the surface of ZIS and subsequently produce •OH. Both these species can cause the degradation of TC. At the same moment, the strongly oxidized holes on g-C_3N_4 also take part in the degradation process of TC molecules. These effects attributed to the generation of oxidizing species, as detailed in the mechanism, are consistent with the observed results from ESR and trapping experiments.

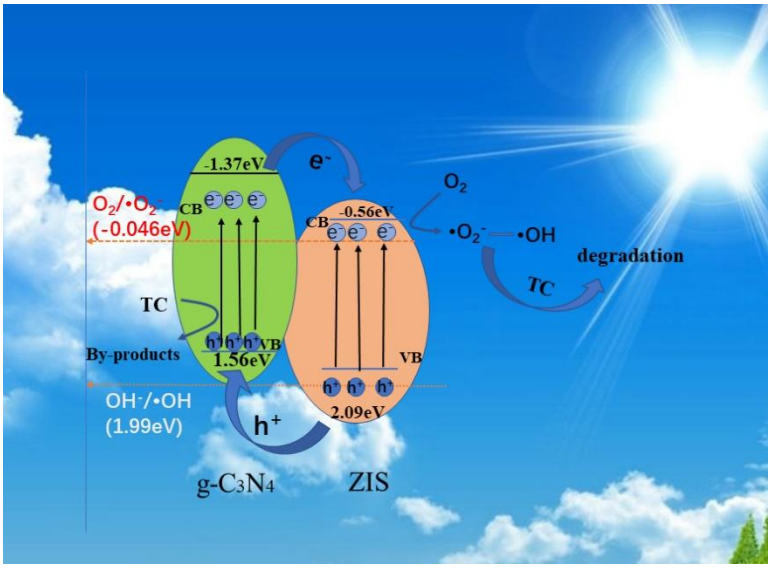

Figure 9. Possible photocatalytic degradation schematic of the g-C_3N_4 (0.5 wt.%)/ZIS composite.

4. CONCLUSIONS

In brief, a one-step hydrothermal path for the decoration of optimized amounts of g-C_3N_4 on

$Zn_3In_2S_6$ microspheres was reported firstly. The catalysis effect of those g-C_3N_4/ZIS samples was discussed by light photocatalytic degradation of TC in detail. Experimental results revealed the composites (specifically, g-C_3N_4 (0.5 wt.%)/ZIS) had remarkably enhanced photocatalytic activity when compared with pure $Zn_3In_2S_6$ and g-C_3N_4. In addition, the g-C_3N_4 (0.5 wt.%)/ZIS composite displayed excellent photostability. Thus, results from the present research may give a brand-new blue print to explore highly efficient and compatible photocatalysts for natural remediation and other potential prospective adhibition.

ACKNOWLEDEGMENT
The research was financially supported by the Shanghai Environmental Protection Engineering Research Center (13dz120703, 14dz1200200), and Project of Shanghai Research and Development Base (11dz2281700).

References

1. C. Su, Y. Lu, Q. Deng, S. Chen, G. Pang, W. Chen, M. Chen, Z. Huang, *Ecotox. Environ. Safe.,* 177 (2019) 39.
2. Y. Wang, H. Zhang, J. Zhang, C. Lu, Q. Huang, J. Wu, F. Liu, *J. Hazard. Mater.*, 192 (2011) 35.
3. B. Luo, D. Xu, D. Li, G. Wu, M. Wu, W. Shi, M. Chen, *ACS. Appl. Mater. Inter.*, 7 (2015) 17061
4. A.H. van Hoek, D. Mevius, B. Guerra, P. Mullany, A.P. Roberts, H.J. Aarts, *Front. Microbiol.,* 3 (2011) 1.
5. H. Chen, X. Bai, Y. Li, L. Jing, R. Chen, Y. Teng, *Sci. Total. Environ.,* 679 (2019) 88.
6. K. Klaus, *Chemosphere.,* 75 (2009) 417.
7. D. Wang, L. Liu, Z. Qiu, Z. Shen, X. Guo, D. Yang, W. Liu, M. Jin, J. Li, *Water. Res.*, 92 (2016) 188.
8. S. Schmidt, J. Winter, C. Gallert, *Arch. Environ. Con. Tox.,* 63 (2012) 354.
9. C. Sean, G. Mike, S. Pernilla, E. Brian, *Sci. Total. Environ.,* 676 (2019) 222.
10. K. He, A D. Soares, H. Adejumo, M. McDiarmid, K. Squibb, L. Blaney, *J. Pharm. Biomed. Anal.,* 106 (2015) 136.
11. M. Mehrjouei, S. Muller, D. Moller, *Chem. Eng. J.,* 263 (2015) 209.
12. C. Gadipelly, A. Pérez-González, G.D. Yadav, I. Ortiz, R. Ibanez, V.K. Rathod, K.V. Marathe, *Ind. Eng. Chem. Res.*, 53 (2014) 11571
13. X. Gou, F. Cheng, Y. Shi, Z. Li, S. Peng, J. Chen, P. Shen, *J. Am. Chem. Soc.*, 128 (2006) 7222.
14. F. Fang, L. Chen, Y. Chen, L. Wu, *J. Phys. Chem. C.*, 114 (2010) 2393.
15. Z. Chen, D. Li, W. Zhang, Y. Shao, T. Chen, M. Sun, X. Fu, *J. Phys. Chem. C.*, 113 (2009) 4433.
16. Z. Lei, W. You, M. Liu, G. Zhou, T. Takata, M. Hara, K. Domen, C. Li, *Chem. Commun*., 17 (2003) 2142.
17. Y. Jiang, Z. Peng, S. Zhang, F. Li, Z. Liu, J. Zhang, Y. Liu, K. Wang, *Ceram int*, 44 (2018) 6115.
18. J. Zhang, S. Meng, X. Ye, C. Ling, S. Zhang, X. Fu, S. Chen, *Appl. Catal. B-Environ.*, 218 (2017) 420.
19. G. Marcì, E. I. García-López, L. Palmisano. *Catal. Today.,* 315 (2018) 126.
20. Y. Wang, M. Qiao, J. Lv, G. Xu, Z. Zheng, X. Zhang, Y. Wu, *FULLER. Nanotub. Car. N.*, 26 (2018) 210.
21. M.P. Reddy, A. Venugopal, M. Subrahmanyam, *Appl. Catal. B-Environ.*, 69 (2007) 164.
22. P. Baskaran, A. Chinnadurai, J.Venkatesan, C.Siva, M. Rathinam, M. Alagiri, *Mat. Sci. Semicon. Proc.,* 100 (2019) 87.
23. Y. Liu, X. Xu, J. Zhang, H. Zhang, W. Tian, X. Li, H. Sun, S. Wang, *Appl. Catal. B-Environ.*, 239

(2018) 334.
24. M. Vlastimil, S. Marcel, R. Martin, M. Alexandr, K. Kamila, K. Martin, P. Petr, *Mat. Sci. Semicon. Proc.,* 100 (2019) 113.
25. W. Zou, B. Deng, X. Hu, Y. Zhou, Y. Pu, S. Yu, K.Ma, J. Sun, H. Wan, L. Dong, *Appl. Catal. B-Environ.*, 238 (2018) 111.
26. L. Liang, Y. Cong, L. Yao, F. Wang, L. Shi, *Mater Res Express.*, 5 (2018) 115510.
27. C. Liu, S. Dong, Y. Chen, *Chem. Eng. J.,* 371 (2019) 706.
28. J. Meng, X. Wang, X. Yang, A. Hu, Y. Guo, Y. Yang, *Appl. Catal. B-Environ.*, 251 (2019) 168.
29. W. Lai, C. Chen, X. Ren, I.-S. Lee, G. Jiang, X. Kong. *Mat. Sci. Eng. C.,* 62 (2016) 166.
30. M. Niu, R. Zhu, F. Tian, K. Song, G. Cao, O. Feng, *Catal. Today.*, 258 (2015) 585.
31. T. Xu, R. Zou, X. Lei, X. Qi, Q. Wu, W. Yao, Q. Xu, *Appl. Catal. B-Environ.*, 245 (2019) 662.
32. J.J. Calvente, R. Andreu, E. Roldan, M. Dominguez, *J. Electroanal. Chem.*, 390 (1995) 115.
33. K.S. Sing, *Pure Appl. Chem.,* 57 (1985) 603.
34. Z. Chen, Y. Xu, *ACS. Appl. Mater. Inter.*, 5 (2013) 13353.
35. C. Tan, G. Zhu, M. Hojamberdiev, K.S. Lokesh, X. Luo, L. Jin, J. Zhou, P. Liu, *J. Hazard. Mater.*, 278 (2014) 572.
36. L. Yuan, M. Yang, Y. Xu, *J. Mater. Chem. A.,* 2 (2014) 14401.
37. Q. Liu, H. Lu, Z. Shi, F. Wu, J. Guo, K. Deng, L. Li, *ACS. Appl. Mater. Inter.*, 6 (2014) 17200.
38. H. Xu, Y. Jiang, X. Yang, F. Li, A. Li, Y. Liu, J. Zhang, Z. Zhou, L. Ni, *Mater. Res. Bull.,* 97 (2018) 158.
39. X. Yuan, D. Shen, Q. Zhang, H. Zou, Z. Liu, F. Peng, *Chem. Eng. J.,* 369 (2019) 292.
40. N. Li, G. Liu, C. Zhen, F. Li, L. Zhang, H. Cheng, *Adv. Funct. Mater.,* 21 (2011) 1717.
41. H. Wang, X. Yuan, Y. Wu, G. Zeng, W. Tu, C. Sheng, Y. Deng, F. Chen, J.W. Chew, *Appl. Catal. B-Environ.,* 209 (2017) 543.
42. Y. Wu, H. Wang, Y. Sun, T. Xiao, W. Tu, X. Yuan, G. Zeng, S. Li, J.W. Chew, *Appl. Catal. B-Environ.,* 227 (2018) 530.
43. M. Sadakane, K. Sasaki, H. Kunioku, B. Ohtani, W. Ueda, R. Abe, *Chem. Commun. (Camb).,* 48 (2008) 6552.